

Image Demosaicing: A Systematic Survey

Xin Li^a, Bahadır Gunturk^b and Lei Zhang^c

^aLane Dept. of Computer Science and Electrical Engineering, West Virginia University

^bDept. of Electrical and Computer Engineering, Louisiana State University

^c Dept. of Computing, The Hong Kong Polytechnic University

ABSTRACT

Image demosaicing is a problem of interpolating full-resolution color images from so-called color-filter-array (CFA) samples. Among various CFA patterns, Bayer pattern has been the most popular choice and demosaicing of Bayer pattern has attracted renewed interest in recent years partially due to the increased availability of source codes/executables in response to the principle of “reproducible research”. In this article, we provide a systematic survey of over seventy published works in this field since 1999 (complementary to previous reviews^{22,67}). Our review attempts to address important issues to demosaicing and identify fundamental differences among competing approaches. Our findings suggest most existing works belong to the class of sequential demosaicing - i.e., luminance channel is interpolated first and then chrominance channels are reconstructed based on recovered luminance information. We report our comparative study results with a collection of eleven competing algorithms whose source codes or executables are provided by the authors. Our comparison is performed on two data sets: Kodak PhotoCD (popular choice) and IMAX high-quality images (more challenging). While most existing demosaicing algorithms achieve good performance on the Kodak data set, their performance on the IMAX one (images with varying-hue and high-saturation edges) degrades significantly. Such observation suggests the importance of properly addressing the issue of mismatch between assumed model and observation data in demosaicing, which calls for further investigation on issues such as model validation, test data selection and performance evaluation.

1. INTRODUCTION

Consumer-level digital cameras were introduced in mid-1990s; in about a decade, the digital camera market has grown rapidly to exceed film camera sales. Today, there are point-and-shoot cameras with over 8 million pixels; professional digital SLR cameras with more than 12 million pixels are also available. Resolution, light sensitivity, and dynamic range of the sensors have been significantly improved such that image quality of digital cameras has become comparable to that of film cameras. During an image capture process, a digital camera performs various processing including auto-focus, white balance adjustment, color interpolation, color correction, compression and more. An important component of the imaging pipeline is color filter array (CFA) interpolation - i.e., to recover an full-resolution image from its CFA data.

Why do we need CFA in color imaging? To produce a color image, there should be at least three color samples at each pixel location. One approach is to use beam-splitters along the optical path to project the image onto three separate sensors as illustrated in Figure 1. Using a color filter in front of each sensor, three full-channel

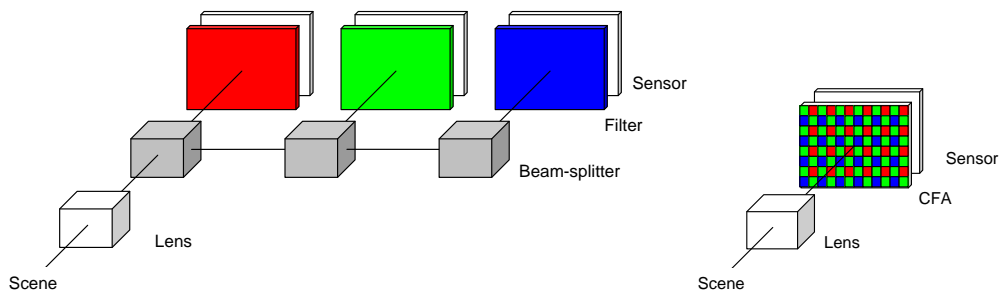


Figure 1. Illustration of optical paths for multi-chip (left) and single-chip (right) digital cameras.

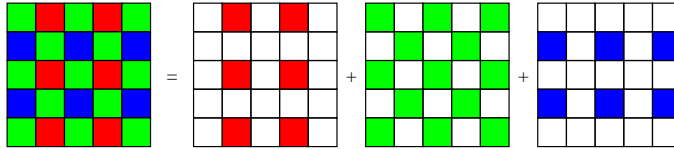


Figure 2. Bayer pattern used in single-chip digital cameras (US Patent3971065).

color images are obtained. This is a costly approach as it requires three charge-coupled device (CCD) sensors and moreover these sensors have to be aligned precisely (a nontrivial challenge to mechanical design). A more cost-effective solution is to put a color filter array (CFA) in front of the sensor to capture one color component at a pixel and then interpolate the missing two color components.²² Because of the mosaic pattern of the CFA, this interpolation process has been widely known as “demosaicing”.

Among many CFA patterns, the most commonly used is the Bayer pattern⁴ (refer to Fig. 2). The Bayer pattern measures the green image on a quincunx grid (half of the image resolution) and the red and blue images on rectangular grids (quarter of the image resolution). The green channel is measured at a higher sampling rate than the other two because the peak sensitivity of the human visual system (HVS) lies in the medium wavelengths, corresponding to the green portion of the spectrum. Although we limit our discussion to the demosaicing problem with reference to the Bayer pattern here, the demosaicing algorithms developed for Bayer pattern can in general be extended to other patterns. Systematic analysis and comparison of different CFA patterns are referred to recent works.^{26, 27}

2. PROBLEM FORMULATIONS

Intuitively image demosaicing can be best understood as an extension of image interpolation for grayscale images. If we denote full-resolution color image by $S = (R, G, B)$ and its Bayer pattern by $z_S = (z_R, z_G, z_B)$, demosaicing includes two inter-related interpolation problems: quincunx interpolation (reconstruct the missing half amount of G pixels) and rectangular interpolation (reconstruct the missing three-quarters of R/B pixels). Although each problem can be solved by the standard image interpolation techniques (e.g., bilinear/bicubic interpolation, edge-directed interpolation⁴²), the real challenge in demosaicing lies in joint exploitation of both intra and inter-channel dependencies such that smaller reconstruction errors can be achieved.

2.1. Statistical Formulation in the Spatial Domain

Modeling inter-channel correlation has been empirically done in several works (e.g., wavelet-domain,²¹ spatial-domain⁴⁰). The empirical findings in those works can be summarized into a constant-hue assumption made by the majority of existing demosaicing algorithms. In color science,¹⁷ hue is among the three main attributes of perceived color (along with lightness and saturation). Hue is often defined by the ratio of color-difference. In the constant-hue assumption, the dependency across color channels is characterized by the smoothness of color-difference or color-ratio functions. Although this heuristics has been extensively used in the literature, it is important to note that the validity of constant-hue assumption heavily depends on the data set (we will elaborate on this matter in experimental result of Section 4).

Under a Bayesian framework,⁵ we can relate the posterior distribution $P(S|z_S, \mathcal{H})$ to the likelihood (imaging) model $P(z_S|S, \mathcal{H})$ and the prior model $P(S|\mathcal{H})$ by the Bayesian formula (\mathcal{H} stands for an assumed model⁵²)

$$P(S|z_S, \mathcal{H}) = \frac{P(z_S|S, \mathcal{H})P(S|\mathcal{H})}{P(z_S|\mathcal{H})}. \quad (1)$$

It is easy to accommodate various uncertainty factors into such statistical formulation. For example, noise interference can be incorporated into the likelihood term (various MMSE-based formulation such as^{11, 64, 69, 70} can be understood from this viewpoint). By contrast, it is the image prior term $P(S|\mathcal{H})$ that reflects our knowledge about spectral-spatial correlation. Just like many other image-related inverse problems, the build-up of prior model $P(S|\mathcal{H})$ often plays the most important role in solution algorithms especially the tradeoff between the cost and the performance.

One convenient strategy is to simply ignore the inter-channel correlation and model each channel independently - e.g., using Markov Random Field⁵⁷ or natural image statistics.⁶⁰ Despite its simplicity, considering intra-plane correlation only still represents one hypothesized model \mathcal{H}_{intra} . Another popular strategy is often to decompose $P(S)$ into the product of $P(G)$ and $P(R, B|G)$; then $P(R, B|G)$ can be further simplified into $P(R|G)P(B|G) = P(d_{RG})P(d_{BG})$ where $d_{RG} = R - G, d_{BG} = B - G$ are inter-channel differences. Such simplified modeling of joint probability distribution function (PDF) in a sequential fashion is denoted by $\mathcal{H}_{inter}^{seq}$ in this paper and it is at the foundation of many existing demosaicing algorithms. It is also possible to model inter-channel correlation in a parallel or iterated fashion (we denote it by $\mathcal{H}_{inter}^{para}$).

2.2. Deterministic Formulation in the Frequency Domain

An alternative formulation of demosaicing is to view CFA data as down-sampling from full-resolution color channels $S = (R, G, B)$.^{2, 14, 15, 19, 29, 43} Full-resolution image is converted to a mosaiced observation z according to the CFA sampling pattern:

$$z = \sum_{S=R,G,B} z_S = \sum_{S=R,G,B} M_S S \quad (2)$$

where z_R, z_G, z_B are the subsampled color channels, and the mask M_S takes a color sample at a pixel according to the CFA pattern. For example, at a red pixel location, $[M_R, M_G, M_B]$ is $[1, 0, 0]$. The masks are explicitly written for a Bayer CFA in terms of cosine functions²:

$$\begin{aligned} z_R(i, j) &= M_R(i, j)R(i, j) = \frac{1}{4} (1 - \cos \pi i) (1 + \cos \pi j) R(i, j) \\ z_G(i, j) &= M_G(i, j)G(i, j) = \frac{1}{2} (1 + \cos \pi i \cos \pi j) G(i, j) \\ z_B(i, j) &= M_B(i, j)B(i, j) = \frac{1}{4} (1 + \cos \pi i) (1 - \cos \pi j) B(i, j) \end{aligned} \quad (3)$$

where (i, j) indicate the pixel coordinates, starting with $(0,0)$. Figure 2 illustrates the CFA image z and the sampled components z_R, z_G , and z_B .

A major advantage of analyzing demosaicing problem in the frequency domain is the rich tools we have in the traditional DSP literature. For example, filter-bank theory⁷³ lends itself to the analysis of demosaicing problem.^{14, 15, 25} Taking another example, it is shown in a recent work⁴³ that the Fourier Transforms (FT) of down-sampled signals (z_R, z_G, z_B) are scaled and periodic replications of the FTs of full-resolution images (R, G, B) though the aliasing in R/B is more severe than that in G (refer to Eqs. (5)-(7) and Fig. 4 of recent paper⁴³). Therefore, several ‘‘conventional’’ designs of anti-aliasing filters for luminance and chrominance components have led to highly-competent performance on Kodak PhotoCD data set with modest computational cost. Frequency-domain formulation can also be extended into any CFA pattern.¹²

So which formulation is better? In our opinion, either statistical or deterministic approach has its own tradeoff. Just like that constant-hue assumption might fall apart when inter-channel correlation gets weak, cross-channel aliasing in the frequency domain could defy any attempt of designing linear filters. Similar to the risk of over-fitting the data in a deterministic setting, some kind of approximation is often inevitable in the pursuit of prior model in statistical setting. It is the matching between theoretical models and observation data as well as practical resource constraints (e.g., memory and computational cost) that determines the appropriate approach. The objective of this review is not to judge which algorithm in which setting is better than others (though we do report extensive simulation results) but to elucidate the similarity and discrepancy among them so an improved understanding about the demosaicing problem could follow.

3. DEMOSAICING METHODS

Single-channel interpolation methods treat each channel separately without utilizing any inter-channel correlation. Standard image interpolation techniques, such as bilinear/bicubic interpolation⁷⁶ and spline interpolation.⁶⁵ When linear interpolation techniques are used, they have a convenient frequency-domain interpretation because the corresponding low-pass filters suppress the aliasing by eliminating overlapped high-frequency components. Since intra-channel interpolation (class \mathcal{H}_{inter}) totally ignores the potential inter-channel correlation, it is likely

to be suboptimal. The natural question is therefore how to improve the quality of demosaiced images by effectively exploiting inter-channel dependency. The most popular class of techniques in the demosaicing literature appears to be sequential interpolation (class $\mathcal{H}_{inter}^{seq}$).

3.1. Sequential Demosaicing Methods

The key motivation behind sequential approach is that the luminance (G) channel is less aliased than the other two. Therefore, having a full-resolution luminance (G) channel facilitates the recovery of chrominance (R/B) ones. Apparently, the accuracy of the first step is critical to the overall performance because of notorious error propagation in sequential approaches. Therefore, significant effort has been devoted to improve the accuracy of luminance (G) channel interpolation in both spatial and frequency domains.

3.1.1. Luminance (Green) Channel Interpolation

A. Spatial-domain approaches

In early works^{1,24,28,36}, missing data in G channel are interpolated by heuristic edge-directed rules. The local edge direction is estimated from available G²⁴ (a local 3×3 window) or R/B³⁶ (a local 5×5 window) or both²⁸ where the second-order gradients of chrominance channels can also be used as correction terms.⁵³ In view of the importance of G channel, more sophisticated edge-directed/sensitive interpolation methods appeared later. For example, local covariance can be estimated based on geometric duality and used to adapt the interpolation.⁴² A closely related work appears in demosaicing by optimal recovery⁵⁸ which formulates the interpolation of G channel by a patch-based quadratic optimization problem. Spatial adaptation can also be achieved by calculating Jacobian matrix of the color map and neighborhood voting.³⁰ In another sophisticated scheme,⁴⁶ missing G pixels are interpolated by weighted sum where local gradients of both G and R/B channels affect the weight assignments.

Interpolation based on explicit edge direction estimation also exist in the literature. In primary-consistent soft-decision (PCSD) scheme,⁷⁵ G pixels are first tentatively interpolated along horizontal/vertical directions and then selected based on a larger context; this scheme is further improved in a later work⁷⁹ where a linear MMSE based strategy is developed to softly fuse instead of select interpolation results along two directions. This line of idea is further refined in.⁷¹ Other similar ideas on edge-sensing adaptive interpolation also exist.^{38,49} In addition to considering H/V directions, fine-granular (as many as 12) directions are used to achieve more accurate edge-adaptive interpolation³² (this idea extends the previous work⁶ and is also adopted by a later work⁷). Most recently, special attention is paid to the class of narrow/line edges^{37,74} which often give rise to artifacts in demosaiced images. It has also been shown that second-order statistics (e.g., variance of color differences) could lead to improved accuracy.^{9,79}

B. Frequency-domain approaches

Deterministic formulation in Eq. (3) suggests the feasibility of recovering missing data through frequency-domain filtering (refer to Fig. 3). In an early frequency-domain approach,¹⁹ ad-hoc diamond-shape low-pass (LP) filter is applied to reconstruct G channel. Later, a wavelet-based green channel update method²¹ is developed based on stronger inter-channel correlation of high-frequency band coefficients. In a more recent work,² the CFA-sampled image is reorganized into luminance and chrominance components and appropriate filters are designed for luminance and chrominance components respectively (luminance channel adopts a specially designed 11×11 filter). Further improvements on anti-aliasing filter design appeared.^{14,15} In another parallel work, frequency-domain filters are designed for horizontal and vertical directions respectively and combined by a local homogeneity criterion.²⁵ Most recently, wavelet-domain edge estimation⁵⁵ is proposed to improve the reconstruction of luminance channel.

In the latest work,⁴³ another extension of frequency-domain demosaicing² is presented where adaptive filtering (AF) is applied on the luminance component. The luminance values at green locations are estimated using a filter similar to the one in²; while the values at red/blue locations are estimated as a weighted sum of neighboring luminance values, where the weights are selected according to the horizontal and vertical gradients (edge indicators). Experimental results in the original paper⁴³ as well as in this work (refer to Section 4) have shown significantly improved performance over previous frequency-domain methods and even outperformed

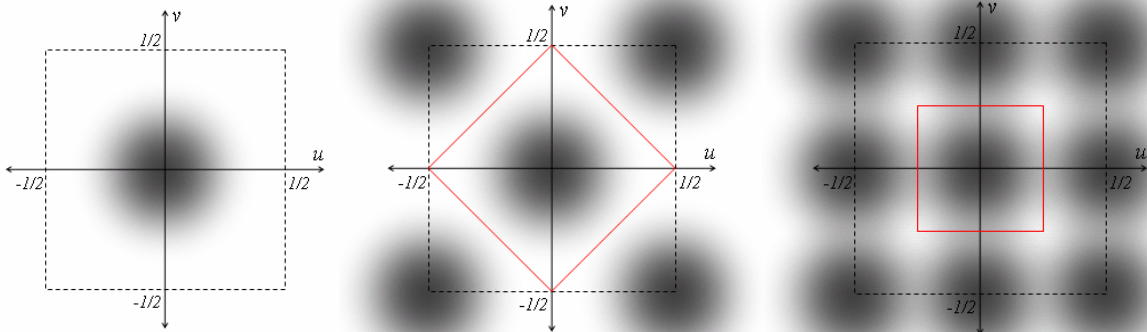


Figure 3. Frequency domain analysis of CFA sampling. Left: Suppose this is the frequency spectrum of the red, green, and blue channels. Middle: Frequency spectrum of the sampled green channel. Right: Frequency spectrum of the red/blue channels. Note that while there is no aliasing for the green channel, red and blue channels are aliased. The green channel can be fully recovered with a low-pass filter whose pass-band is outlined in the middle figure. For the red/blue channels, such a low-pass filtering operation cannot eliminate the aliasing.

several state-of-the-art demosaicing techniques on Kodak PhotoCD images at a modest computational cost. However, such adaptive luminance filtering does not admit equivalent frequency-domain interpretation any more and implicitly suggests the superiority of spatially adaptive interpolation.

3.1.2. Chrominance (Red/Blue) Channel Interpolation

In sequential demosaicing, one commonly used assumption is that the *hue* (color ratios or differences) within an object in an image is constant. Although this assumption only holds within the boundary of an object, it has been extensively used for the interpolation of the chrominance (red and blue) channels.^{1, 10, 18, 36, 62} This class of *constant-hue* based interpolation techniques have shown good performance on Kodak PhotoCD data set which were originally scanned from film-based photos. For data set with higher-quality, the constant-hue assumption becomes less valid and consequently render larger reconstruction errors. In parallel to luminance interpolation, we organize chrominance interpolation techniques into spatial and frequency domain respectively.

A. Spatial-domain approaches

Based on the interpolated full-resolution G channel, the chrominance (R/B) channels are then reconstructed by enforcing constant-hue rules. Specifically, color-difference signals $d_{RG} = R - G$, $d_{BG} = B - G$ are interpolated based on full-resolution G channel and down-sampled R/B channels; then G channel is simply added back to two color-difference channels for recovering R/B. In early works, color-ratio¹⁰ or color-difference⁶² interpolation is often implemented by standard linear interpolation. A normalized model⁴⁸ has also been proposed for color-ratio based demosaicing. The basic idea is to introduce a nonzero bias β to the color ratio rule - i.e., $\frac{R_i + \beta}{R_j + \beta} = const.$ It has been shown that adjusting the parameter β could lead to improved performance over original rule ($\beta = 0$).

Another so-called vector spectral model⁵⁰ based on collinear relationship of spatially-adjacent (R, G, B) vectors was developed later. Edge-directed interpolation has also been extended for interpolating R/B channels as well⁴⁶ and similar idea can also be used to improve the interpolation of color-difference signals⁵⁴ (especially R/B pixels at B/R locations). In a recent work, interpolation of R/B channels is further adapted based on direction similarity measurement.⁷⁷ Similar advanced spatially-adaptive strategies also exist in other works.^{16, 34, 72} Generally speaking, lower errors can be achieved at the price of increased computational cost due to spatial adaptation.

B. Frequency-domain approaches

Reconstruction of chrominance channels can also be implemented by designing anti-aliasing filters in the frequency domain. In the simplest case, bilinear filters are used to recover chrominance channels $R-L, G-L, B-L$

(L denotes the luminance channel).² Improved linear filters for chrominance channels are developed^{14,15} to reduce the spectral crosstalk. Similar linear interpolation strategies are also used in more recent frequency-domain methods.^{25,43} It has been widely observed that reconstruction errors in R/B channels are often significantly larger than those in G channel due to more severe aliasing. However, as reported in the latest work,⁴³ adaptive filtering applied to chrominance channels improves the performance marginally at the price of much higher computational cost.

Another effective approach of interpolating missing data in chrominance channels is to borrow wavelet theory. Based on the observation that edges across color channels are highly correlated, it is possible to obtain a good estimation of high-frequency band coefficients in chrominance from their luminance counterpart by simple max rule¹³ or mean-corrected synthesis.⁸ More systematic approach is based on projection-onto-convex-set (POCS) theory.²¹ By alternating the projection onto observation and detail constraint sets, chrominance channels can be efficiently reconstructed after few iterations. Since POCS-based demosaicing achieves good performance at the price of moderate computational cost, it has been widely used as the benchmark scheme for later works.

3.1.3. Postprocessing/refinement Techniques

If the assumed model \mathcal{H}_{inter} well matches the image data, there would be no need for any further processing. The unfortunate consequence of mismatch is visibly annoying artifacts (e.g., false color, zipper artifacts and so on). Even at the absence of artifacts, edge blurring could be another plague due to the LP properties of various interpolation filters. Accordingly, several post-processing techniques have been proposed as a salvage strategy for either enhancing the sharpness of edges or suppressing undesirable artifacts. In an early work,¹⁸ median filtering was proposed to process inter-channel differences of the demosaiced images. This idea was later extended into vector median filtering⁴⁶ based on the observation that filtering inter-channel differences separately does not take the spectral correlation into account. Another extension based on median filtering idea appeared in more recent works.^{25,56}

In one of the pioneering work on demosaicing,³³ inverse diffusion based on extending Gabor’s filter is used to generate coherence-enhancing flow, which yields images with more pleasant visual quality (not necessarily lower MSE). In another relatively early attempt,⁵⁷ a markov random field (MRF) model is applied to demosaiced images to improve the reconstruction of edges. Bilateral filtering techniques has also been proposed for demosaicing.⁶⁶ A color-ratio based post-processing technique is developed and has demonstrated effective for suppressing the artifacts in demosaiced images by various algorithms.⁴⁷ Artifacts suppression can also be implemented in the frequency domain⁵⁴ because various artifacts often occur in high-frequency components.

3.2. Other demosaicing methods

Despite the popularity of sequential demosaicing, it has a fundamental weakness of error propagation - any errors rendered during the interpolation of the luminance (G) channel would inevitably propagate to the chrominance channels. Based on the observation that refinement of luminance and chrominance channels can be mutually beneficial, it is possible to alleviate the problem of error propagation by iterative reconstruction. In an early work of iterative demosaicing,³³ G and R/B channels are iteratively refined based on color-ratio rule; a computationally more efficient iterative demosaicing method using color-difference rule is proposed in successive approximation (SA) scheme⁴⁰ and later extended by incorporating edge-weighted interpolation.⁶⁸

An alternative approach is to simultaneously model the three color channels (class $\mathcal{H}_{inter}^{para}$). Inspired by the effectiveness of vector median filter³ in color image processing, a vector CFA demosaicing algorithm²³ was proposed. It is also possible to take a learning-based approach towards demosaicing - i.e., assuming some training data is available, we can reconstruct full-resolution images by “learning” the relationship between CFA pattern and their surrounding pixels. The earliest use of neural networks for demosaicing appeared in 2000.^{20,31} Training data can also used to classify local image features.³⁵ Multiple neural networks⁴⁴ specialized in learning nonlinear spatial correlations at various gradients and directions are developed. A novel vector-quantization (VQ) based approach towards demosaicing was proposed recently.⁵⁹

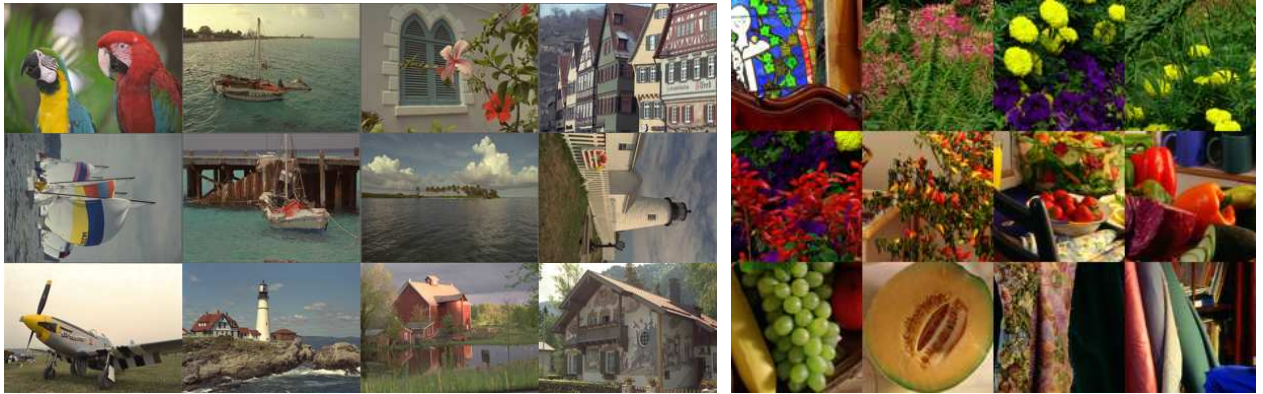


Figure 4. Kodak PhotoCD image set (left) and cropped IMAX image set (right).

3.3. Performance Evaluation of Demosaicing Algorithms

Performance evaluation of demosaicing algorithms was first systematically studied by several psychologists.⁴⁵ A commonly used quantitative measure for evaluating demosaicing algorithms is mean square error (MSE) or equivalently peak signal to noise ratio (PSNR) ($PSNR = 10 \log_{10} \frac{255^2}{MSE} (dB)$). In some works,^{47, 51} mean absolute difference (MAD) and normalized color difference (NCD)⁶³ are also used as supplementary criterion. It is also argued that Euclidean distances in the perceptually uniform CIELab and CIELuv spaces and the s-CIELab⁸⁰ are better measures considering the human visual perception. Therefore, we have seen an increased number of paper using s-CIELab metric in their performance comparison.^{40, 43, 46, 61}

All those objective measures assume the availability of a reference image. Unfortunately, such assumption does not always hold since the output of any digital camera has already been processed by a pipeline including optical low-pass filtering and demosaicing. Since different cameras may have different demosaicing algorithms, some bias is inevitable, which deviate from the ground-truth (an image acquired from 3CCD camera). To the best of our knowledge, computer-based simulation has been used in all published works on demosaicing - i.e., full-resolution color images acquired from single-CCD cameras are first down-sampled according to a specific CFA pattern and then the reconstructed images are compared with the “original” quantitatively. The only justification we have for this approach is that the original full-resolution color images do visually appear pleasant (therefore can be used as the reference even if they have been through processing pipeline). However, we might get away from this pitfall if a no-reference (blind) quality assessment³⁹ method can be developed for color images.

4. EXPERIMENTAL RESULTS

In this section, we report experimental results of our comparative study among eleven selective inter-channel demosaicing algorithms on two different benchmark data sets. The ten demosaicing algorithms are: 1) Lu&Tan’s method (LT)⁴⁶; 2) alternating projection (AP)²¹; 3) adaptive homogeneity-directed (AHD)²⁵; 4) successive approximation (SA) with edge-weighted improvement⁶⁸; 5) Lukac’s CCA method⁵¹ with post-processing⁴⁷; 6) frequency-domain (FD) demosaicing²; 7) Directional Filtering and a posteriori Decision (DFPD)⁵⁴; 8) Variance of color-difference (VCD)⁹; 9) Directional Linear Minimum Mean Square-Error Estimation (DLMMSE)⁷⁹; 10) local polynomial approximation (LPA)⁶¹; 11) Adaptive filtering (AF) for demosaicing.⁴³ We believe they represent the current state-of-the-art in this field and the source codes or executables of all algorithms are made directly available from the original authors.

The two benchmark data sets are Kodak PhotoCD (sized by 512×768) * and IMAX high-quality images (approximately 4M-pel) †. Two metrics (PSNR and S-CIELab measure ΔE_{ab}^*) are calculated as the objective measures for comparing the demosaicing algorithms. Since some implementation skips the processing of pixels at

*Higher-resolution versions of this set are available but the edges appear noticeably smoother.

†due to the large size of those images, we crop out 400×400 regions with high-saturation and varying-hue.

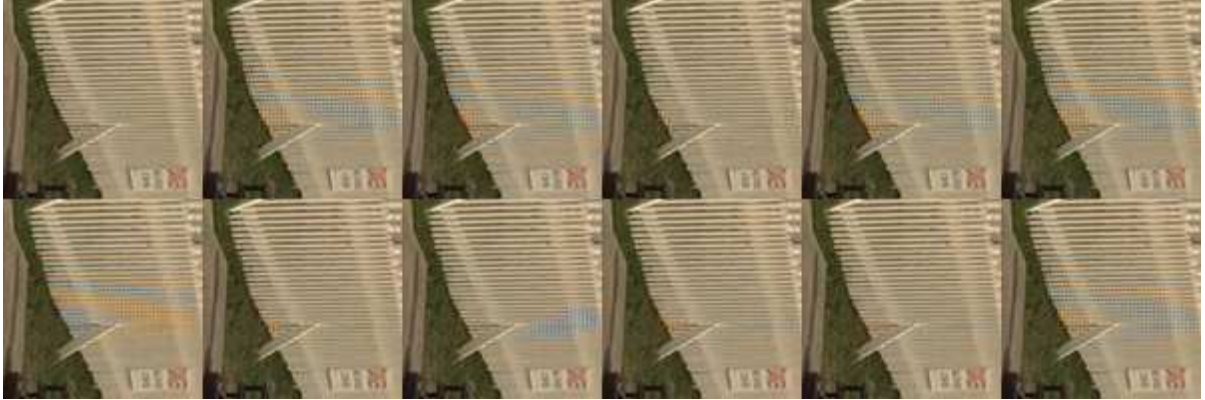


Figure 5. Comparison of *fence* portion of demosaiced images by different algorithms for *img8* (lighthouse): top-down and left-right, original, algorithms 1-11 respectively.

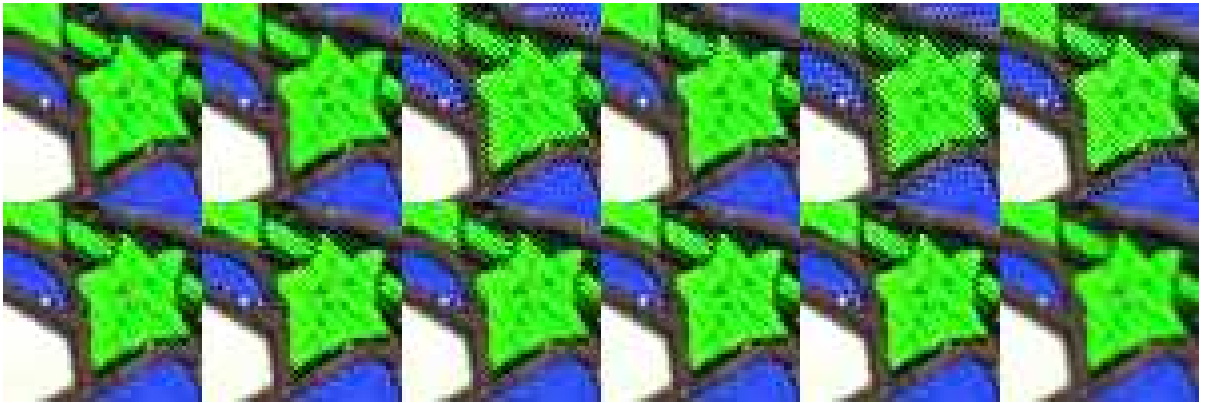


Figure 6. Comparison of high-saturation portion of demosaiced images by different algorithms for *No.1* in IMAX image set: top-down and left-right, original, algorithms 1-11 respectively (algorithm 6 is AF instead of FD and algorithm 11 is NEDI instead of AF).

the border, we exclude those pixels whose distance to the border is fewer than 10 pixels in our calculation. Due to the variation of implementations (e.g., MATLAB vs. C codes), the actual running time does not faithfully reflect the computational complexity of each algorithm. Therefore, we opt not to report complexity-related measures.

Tables I and II include the performance comparison on the Kodak PhotoCD data set. It can be observed that 1) algorithms 8-10 (VCD, DLMMSE and LPA) appear to outperform others by noticeable margin on this image set; while algorithms 3 (AHD) and 6 (FD) fall behind especially on the average PSNR performance; 2) improved frequency-domain method by adaptive filtering (AF) does dramatically improve the performance over previous work (FD); however, such gain appears to largely due to the improvement of luminance channel (essentially it goes back to spatially-adaptive interpolation); 3) S-CIELab measure has a good correlation with PSNR measures but there exist exceptions. For instance, AHD falls behind AP by about $1.6dB$ on average PSNR but outperforms AP in terms of S-CIELab metric; although CCA achieves good PSNR performance, its average S-CIELab errors are the second largest among all (note that post-processing is already activated). Fig. 5 includes the comparison of the fence portion of demosaiced *img8* which is often used to check the visibility of false color artifacts in demosaiced images. We note that algorithms 3,7,9,10 (AHD,DFPD,DLMMSE,LPA) are more artifact-free than others on this specific example.

Despite the popularity of Kodak PhotoCD images, they are relatively low-quality representation of natural world (they are scanned version from film-based photos). Similar to the work,⁴³ we also include another set of IMAX images with higher quality (refer to Fig. 4). The hue and saturation characteristics of IMAX images are

No.	LT	AP	AHD	SA	CCA	FD	DFPD	VCD	DL	LPA	AF
1	42.90	42.07	41.42	41.90	41.14	38.86	42.48	42.97	42.90	43.86	42.93
	46.24	45.33	45.16	46.32	45.56	44.16	46.15	46.74	47.56	47.75	46.98
	43.06	42.69	42.23	42.96	42.13	41.41	43.13	43.50	43.86	44.46	43.65
2	38.00	39.06	38.58	40.21	39.58	37.40	40.27	40.93	41.39	42.10	38.74
	39.82	42.75	40.08	43.48	43.03	42.30	42.04	43.83	43.69	44.81	41.67
	37.59	38.97	38.05	39.54	38.96	38.23	39.68	40.37	40.44	41.07	38.18
3	43.33	42.53	41.13	42.53	41.74	39.35	42.38	42.92	42.95	43.77	43.48
	45.88	44.91	43.67	44.52	45.21	43.49	44.97	45.58	46.26	46.53	46.66
	42.44	41.51	40.33	40.48	40.87	41.03	41.47	41.85	41.80	42.65	42.41
4	34.88	35.20	34.17	35.96	35.65	32.28	35.56	36.57	36.33	37.42	35.51
	37.15	39.66	36.14	40.37	39.77	37.58	38.08	40.25	39.63	41.15	38.88
	34.98	35.58	34.35	36.78	36.22	32.95	35.85	37.10	36.66	37.85	35.63
5	42.85	42.50	41.76	42.93	42.76	39.93	42.86	43.70	43.71	44.26	43.16
	44.90	45.30	44.06	46.12	45.98	43.60	45.44	46.71	46.68	47.01	46.29
	41.90	42.31	41.08	42.33	41.94	41.11	42.49	43.10	42.93	43.42	42.69
6	38.81	39.08	37.64	39.18	39.03	36.88	39.29	39.73	39.98	40.44	39.38
	40.88	42.78	39.89	43.29	43.32	42.74	41.75	43.33	43.19	43.85	42.63
	39.35	40.02	38.41	40.53	40.46	39.23	39.94	40.82	40.96	41.39	39.80
7	41.01	42.18	42.37	43.40	42.45	40.10	43.77	44.47	44.75	44.91	41.61
	42.88	45.75	43.77	46.42	45.72	44.84	45.41	47.03	46.82	47.15	44.53
	40.55	41.70	41.57	42.24	41.62	40.62	42.94	43.55	43.54	43.77	40.99
8	40.11	40.02	39.16	40.98	40.66	37.12	40.56	41.10	41.69	42.18	40.58
	41.95	43.86	40.77	44.33	43.96	42.05	42.55	44.09	44.14	44.72	43.49
	39.46	39.95	38.62	40.33	39.95	37.90	40.15	40.60	40.88	41.46	39.92
9	42.14	41.79	40.22	42.15	42.48	39.78	41.40	42.31	42.77	42.95	42.37
	43.47	44.59	41.66	45.07	45.49	43.59	43.26	44.89	44.88	45.14	44.94
	40.47	40.66	39.01	40.33	40.90	40.41	40.24	40.98	40.95	41.36	40.79
10	38.87	39.51	37.62	40.32	40.71	37.80	38.83	40.21	40.40	40.91	39.61
	40.19	42.79	38.88	43.45	43.75	42.17	40.61	42.89	42.43	43.13	42.16
	38.21	39.07	36.93	39.41	39.60	38.44	38.28	39.41	39.34	39.77	38.77
11	39.20	38.61	37.01	38.54	38.18	37.10	38.33	38.93	39.20	39.37	39.29
	41.40	41.23	39.46	41.56	41.67	40.53	40.91	41.97	42.26	42.32	42.39
	38.65	38.19	36.82	38.13	38.12	37.61	38.22	38.77	38.84	39.10	38.91
12	36.05	36.78	34.58	37.18	36.20	36.89	36.32	37.29	37.99	37.78	36.80
	37.22	39.07	36.49	39.88	39.68	39.83	38.25	39.86	39.87	40.05	39.04
	34.59	35.07	33.90	35.68	35.55	35.65	35.11	35.75	36.22	36.17	35.15
Avg	40.32	40.92	39.36	41.36	41.11	39.58	40.81	41.78	41.89	42.39	41.11

Table 1. PSNR(dB) performance comparison of different demosaicing methods on Kodak PhotoCD image set (DL is short-hand for DLMMSE).

No.	LT	AP	AHD	SA	CCA	FD	DFPD	VCD	DL	LPA	AF
1	0.4760	0.4993	0.5457	0.5058	0.6471	0.6451	0.4984	0.4745	0.4446	0.4170	0.4530
2	0.8884	0.8439	0.7354	0.7732	0.8802	0.8960	0.7393	0.6950	0.6713	0.6535	0.8472
3	0.4925	0.5770	0.6103	0.6336	0.6733	0.7182	0.5654	0.5335	0.5194	0.4696	0.4770
4	1.3261	1.3781	1.2601	1.3226	1.2743	1.6954	1.3070	1.1154	1.1799	1.0735	1.2510
5	0.5436	0.5655	0.5605	0.5414	0.6247	0.6452	0.5617	0.4979	0.4985	0.4857	0.5183
6	0.7436	0.7526	0.7300	0.7180	0.7775	0.8523	0.7157	0.6633	0.6417	0.6238	0.7135
7	0.6593	0.6213	0.5226	0.5761	0.6840	0.7152	0.5416	0.4958	0.4803	0.4784	0.6355
8	0.7344	0.7455	0.7473	0.7144	0.7748	0.8784	0.7507	0.6786	0.6593	0.6300	0.6964
9	0.5277	0.5486	0.5809	0.5399	0.5771	0.5830	0.5822	0.5252	0.4990	0.4905	0.5066
10	0.8536	0.8465	0.8716	0.8050	0.8468	0.9047	0.9020	0.7869	0.7802	0.7655	0.8160
11	0.8679	0.9394	1.0578	0.9736	1.0691	1.0302	0.9483	0.8997	0.8512	0.8577	0.8352
12	0.9479	0.9998	1.0826	1.0228	1.1169	0.9692	1.0305	0.9234	0.8717	0.9562	0.8881
Avg	0.7551	0.7765	0.7754	0.7605	0.8288	0.8777	0.7619	0.6908	0.6748	0.6585	0.7198

Table 2. S-CIELab measure (ΔE_{ab}^*) comparison of different demosaicing methods on Kodak PhotoCD image set.

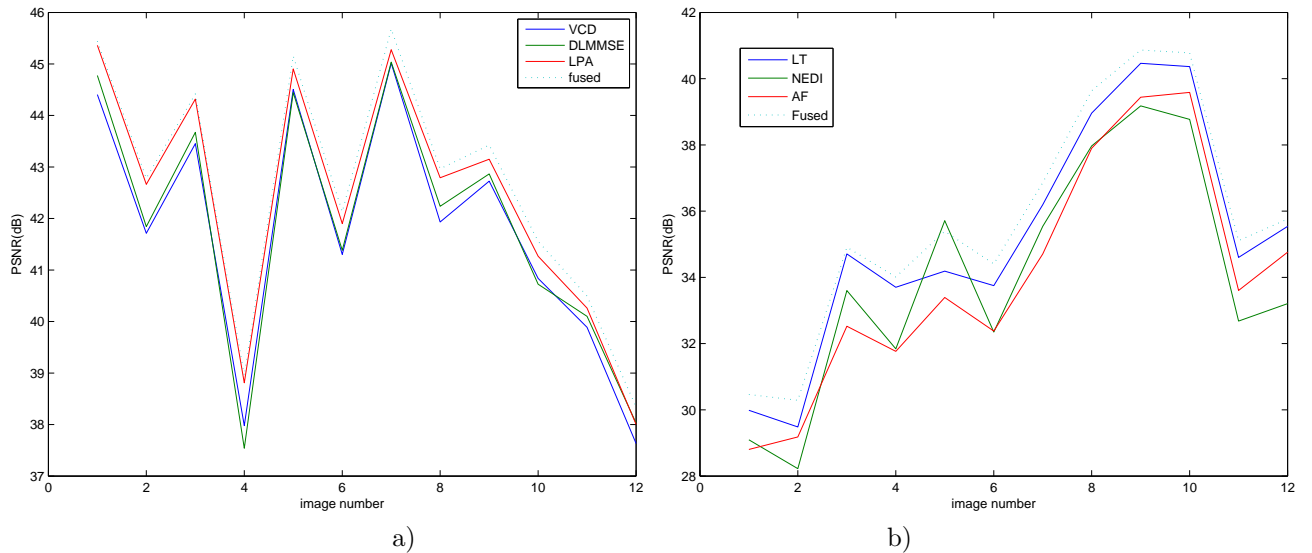


Figure 7. a) Fusion of algorithms 8,9,10 (VCD, DLMMSE and LPA) on Kodak PhotoCD (dashed line - after fusion); b) Fusion of algorithms 1,6,11 (LT, AF and NEDI) on IMAX test images (dashed line - after fusion).

No.	LT	AP	AHD	SA	CCA	AF	DFPD	VCD	DL	LPA	NEDI
1	29.35	26.62	26.91	25.32	26.27	28.56	27.73	28.37	27.92	28.05	27.69
	33.51	27.94	30.45	26.39	28.74	31.22	30.86	30.36	31.39	31.12	32.83
	27.11	25.18	25.12	23.80	24.74	26.63	26.15	26.50	25.88	26.21	26.75
2	27.93	26.60	25.61	25.51	25.84	28.61	27.17	27.21	27.14	25.84	25.59
	32.22	27.55	29.03	26.20	27.70	30.39	29.49	29.18	30.34	27.67	31.96
	28.31	26.96	25.90	26.06	26.11	28.54	27.32	27.52	27.30	26.16	27.13
3	35.41	31.31	32.01	30.23	31.88	33.92	32.42	32.90	33.38	32.92	31.63
	37.51	30.78	33.21	28.99	31.98	33.98	33.75	33.08	34.42	33.51	36.10
	31.21	28.46	27.45	26.67	27.48	29.67	29.03	29.95	28.67	28.88	33.08
4	33.37	30.39	30.79	29.44	30.40	32.03	31.17	31.22	31.98	30.59	28.70
	36.04	30.87	32.85	29.46	31.67	33.41	33.31	32.53	33.77	31.82	34.32
	31.70	29.08	28.06	27.49	27.90	29.85	29.40	30.09	29.27	28.47	32.52
5	30.18	28.63	28.31	26.25	27.97	31.16	29.83	30.01	29.42	30.69	32.38
	39.31	32.13	35.10	29.85	32.34	36.39	35.10	35.13	36.13	36.48	39.97
	33.07	30.52	30.42	28.60	29.72	32.63	31.39	32.30	31.43	32.17	34.79
6	30.70	28.78	28.71	26.81	27.93	30.59	29.63	29.74	29.70	29.68	28.26
	37.23	31.45	33.85	29.46	31.77	34.73	34.16	33.60	34.88	33.61	36.48
	33.32	30.57	30.10	28.88	29.36	31.81	31.03	31.74	31.18	30.66	32.31
7	33.87	31.61	31.93	29.77	30.90	33.35	32.74	32.87	32.82	33.51	32.69
	40.04	34.04	37.17	32.82	34.62	37.47	37.31	36.57	38.04	37.97	40.07
	34.66	31.96	32.08	30.10	31.06	33.30	32.96	33.39	32.84	33.32	33.87
8	36.51	34.13	34.65	33.01	33.68	36.04	35.51	35.93	35.17	36.40	36.16
	42.64	37.14	40.26	37.09	38.04	40.69	40.44	40.07	41.06	41.65	42.67
	37.72	35.39	36.18	34.94	35.35	36.98	36.60	37.02	36.73	37.23	35.08
9	40.12	38.18	38.70	38.00	38.42	39.35	38.66	38.90	39.35	39.55	37.20
	42.95	39.46	40.88	39.53	40.29	41.62	41.04	40.97	41.78	41.94	42.75
	38.32	36.56	36.36	35.92	36.09	37.35	36.87	37.45	36.91	37.39	37.58
10	40.69	38.86	38.69	38.46	38.37	39.63	38.96	39.45	39.58	39.64	38.53
	43.02	40.24	41.13	40.38	40.46	42.06	41.28	41.31	42.07	41.86	42.73
	37.39	36.50	36.15	36.23	36.16	37.06	36.67	36.79	36.82	36.95	35.06
11	33.80	31.81	31.59	30.63	31.18	33.11	32.40	32.57	32.73	32.66	30.83
	37.66	33.53	35.21	32.87	33.58	35.93	35.44	35.07	36.19	35.55	36.72
	32.34	30.85	30.19	29.61	29.99	31.77	31.33	31.46	31.28	31.28	30.50
12	34.43	32.34	33.28	31.26	32.25	33.88	33.81	33.90	33.91	34.14	30.78
	38.85	35.30	37.84	34.81	35.90	37.92	37.77	37.47	38.21	38.05	38.23
	33.33	31.66	31.85	30.66	31.53	32.48	32.48	32.58	32.46	32.61	30.60
Avg	35.16	32.04	32.72	30.87	31.88	34.00	33.37	33.48	33.67	33.51	34.01

Table 3. PSNR(dB) performance comparison of different demosaicing methods on cropped IMAX image set.

arguably closer to those of images acquired by digital cameras of these days. For this data set, we have tested all selected 11 algorithms with one replacement: we replace FD (since AF represents a more competing frequency-domain approach) by new edge-directed interpolation (NEDI)⁴² (an intra-channel interpolation technique). The rationale behind is that we want to include \mathcal{H}_{intra} into our comparison. It can be observed from Tables III and IV that the performance of most existing algorithms degrade a lot on this more challenging data set. Many inter-channel demosaicing do not necessarily outperform NEDI (intra-channel method). It should be noted that the algorithm⁴⁶ has shown impressive performance on this new data set, which suggests the importance of jointly exploiting spatial and spectral correlation and effectiveness of weighted interpolation. Fig. 6 includes the subjective comparison which also demonstrate the problems with several inter-channel demosaicing based on constant-hue assumptions.

No.	LT	AP	AHD	SA	CCA	AF	DFPD	VCD	DL	LPA	NEDI
1	2.3208	3.4122	3.3815	4.4502	3.8320	2.5940	2.7468	2.7935	2.7424	2.7904	2.4820
2	2.8572	3.8968	4.3594	4.9143	4.6421	3.0212	3.3286	3.4767	3.3965	4.6235	3.0562
3	1.2804	2.1808	2.3686	3.0774	2.6078	1.6738	1.7504	1.8299	1.8317	1.9461	1.3955
4	1.3765	2.4275	2.3155	3.1426	2.7003	1.8582	1.8684	2.0322	1.8845	2.4445	1.7296
5	1.8645	2.2549	2.7796	3.5179	3.1754	1.8140	2.0432	2.0454	2.2216	1.7926	1.1788
6	1.6623	2.3187	2.6126	3.1654	2.8622	1.8659	2.0913	2.1105	2.0983	2.2694	1.8370
7	1.2083	1.6204	1.6962	2.2571	2.0230	1.3126	1.3321	1.4045	1.3864	1.2792	1.1664
8	0.8455	1.0618	1.0880	1.2372	1.2615	0.8762	0.8997	0.8997	0.9345	0.8157	0.8036
9	0.6151	0.7660	0.8112	0.8247	0.8608	0.6603	0.7142	0.7159	0.6745	0.6485	0.6503
10	0.8516	1.0161	1.0739	1.0484	1.1042	0.9093	0.9896	0.9674	0.9244	0.9349	0.9187
11	1.2125	1.6191	1.8435	2.0979	1.9946	1.3555	1.3998	1.4629	1.4541	1.5137	1.4444
12	1.1955	1.4461	1.4337	1.8392	1.7616	1.2452	1.2137	1.2518	1.2525	1.2192	1.3898
Avg	1.4408	2.0017	2.1470	2.6310	2.4021	1.5989	1.6982	1.7492	1.7335	1.8565	1.5044

Table 4. S-CIELab measure (ΔE_{ab}^*) comparison of different demosaicing methods on cropped IMAX image set.

The above two experiments suggest that the issue of mismatch between assumed model and observation data has to be properly addressed. One solution to reduce the risk of mismatch is to fuse the demosaicing results by different algorithms. An ad-hoc fusion strategy is to take the average of demosaiced images - despite the simplicity of this strategy, it provides an intuitive approach of studying whether reconstruction errors by different algorithm are independent. Fig. 7 contains the PSNR performance comparison before and after ad-hoc fusion for two data sets. For Kodak PhotoCD, we have chosen to combine the three best algorithms (VCD, DLMMSE and LPA) based on the results in Table I; for IMAX images, we opt to fuse the best inter-channel method (LT) with an intra-channel method (NEDI). It can be seen from Fig. 7 that noticeable PSNR improvement has been achieved by even ad-hoc averaging. More systematic fusion is left for future studies (refer to recent works^{41, 78}).

5. CONCLUSIONS AND FUTURE DIRECTIONS

In this survey article, we have reviewed over seventy papers in the literature of image demosaicing. The majority of existing demosaicing algorithms exploit the spectral correlation by sequential strategies - i.e., the luminance (G) channel is recovered first and then chrominance (R/B) channels are reconstructed based on the full-resolution luminance image. Spatial adaptation based on local deterministic (e.g., gradients) or statistical (e.g., variance/covariance) has shown critical to the performance of various demosaicing techniques. Our comparative studies with eleven very best demosaicing algorithms have demonstrated the importance of jointly exploiting spatial and spectral correlations especially for images with high-saturation and varying-hue. We have also observed that even ad-hoc fusion by averaging different demosaiced images could lead to further improvement.

There are three directions along which further studies are definitely needed. First, demosaicing of images with weak spectral correlation remains a challenging task. Our understanding about the tradeoff between spatial and spectral correlation is still primitive though some attention has been paid to this issue by one group of contributing authors to this session.⁷⁸ Second, more systematic fusion strategy could lead to reduced risk of mismatch between assumed models and observation data. Which models to combine and how to spatially adaptive fuse demosaiced images are importance questions along this line. Last but not the least, the performance evaluation of demosaicing algorithms needs more careful investigation. If the data available to research community are only images acquired by single-CCD cameras, we need to be more cautious about the risk with computer-based simulation. Competing for higher PSNR or lower sCIELAB values would become less meaningful if the used reference image could not faithfully reflect the true characteristics (i.e., color images acquired a 3CCD camera). Without understanding other components in the pipeline (e.g., white balancing and color correction), demosaicing alone might become a pet for academia only and never have any serious impact on the industry of electronic imaging.

REFERENCES

1. J. E. Adams and J. F. Hamilton Jr. Adaptive color plane interpolation in single color electronic camera. U.S. Patent 5 506 619, Apr 1996.
2. D. Alleysson, S. Susstrunk, and J. Herault. Linear demosaicing inspired by the human visual system. *IEEE Trans. on IP*, 14(4):439–449, April 2005.
3. J Astola, P Haavisto, and Y Neuvo. Vector median filtering. *Proceedings of the IEEE*, 78(4):678–689, 1990.
4. B. E. Bayer. Color imaging array, July 1976. U.S. Patent 3971065.
5. D.H. Brainard. Bayesian method for reconstructing color images from trichromatic samples. In *Proceedings of the IS&T 47th Annual Meeting*, pages 375–380, 1994.
6. E. Chang, S. Cheung, and D. Y. Pan. Color filter array recovery using a threshold-based variable number of gradients. *SPIE*, 3650:36–43, 1999.
7. H.A. Chang and Homer H. Chen. Stochastic color interpolation for digital cameras. *IEEE Trans. Cir. Sys. Video Tech.*, 17(8):964–973, Aug. 2007.
8. L. Chen, K.H. Yap, and Y. He. Color filter array demosaicking using wavelet-based subband synthesis. In *Proc. ICIP*, pages II: 1002–1005, 2005.
9. K.-H. Chung and Y.-H. Chan. Color demosaicing using variance of color differences. *IEEE Trans. on IP*, 15(10):2944–2955, Oct. 2006.
10. D.R. Cok. Signal processing method and apparatus for producing interpolated chrominance values in a sampled color image signal. U.S. Patent 4 642 678, Feb 1987.
11. B.C. de Lavarene, D. Alleysson, and J. Herault. Practical implementation of lmmse demosaicing using luminance and chrominance spaces. *CVIU*, 107(1-2):3–13, July 2007.
12. Brice Chaix et al. de Lavarene. Efficient demosaicing through recursive filtering. In *Proc. IEEE Int. Conf. Image Processing*, volume 2, pages 189–192, 2007.
13. J. Driesen and P. Scheunders. Wavelet-based color filter array demosaicking. In *Proc. ICIP*, pages V: 3311–3314, 2004.
14. E. Dubois. Frequency-domain methods for demosaicking of bayer-sampled color images. *IEEE Signal Proc. Letters*, 12(12):847–850, December 2005.
15. E. Dubois. Filter design for adaptive frequency-domain bayer demosaicking. In *Proc. of International Conference on Image Processing*, pages 2705–2708, 2006.
16. S. Moriya et al. Advanced demosaicing method based on the change of colors in a local region. *IEEE Transactions on Consumer Electronics*, 52(1):206–214, Feb. 2006.
17. Mark D. Fairchild. *Color Appearance Models*. Addison Wesley, 1998.
18. W. T. Freeman. Method and apparatus for reconstructing missing color samples. *U.S. Patent 4,774,565*, Sep. 1988.
19. J. W. Glotzbach, R. W. Schafer, and K. Illgner. A method of color filter array interpolation with alias cancellation properties. In *Proc. IEEE Int. Conf. Image Processing*, volume 1, pages 141–144, 2001.
20. J. Go, K. Sohn, and C. Lee. Interpolation using neural networks for digital still cameras. *IEEE Trans. Consumer Electronics*, 46(3):610–616, August 2000.
21. B. Gunturk, Y. Altunbasak, and R. M. Mersereau. Color plane interpolation using alternating projections. *IEEE Transactions on Image Processing*, 11(9):997–1013, 2002.
22. B. K. Gunturk, J. Glotzbach, Y. Altunbasak, R. W. Schafer, and R. M. Mersereau. Demosaicking: color filter array interpolation. *IEEE Signal Processing Magazine*, 22(1):44–54, January 2005.
23. M. R. Gupta and T. Chen. Vector color filter array demosaicing. In M. M. Blouke, J. Canosa, and N. Sampat, editors, *Proc. SPIE*, volume 4306, pages 374–382, May 2001.
24. Robert H. Hibbard. Apparatus and method for adaptively interpolating a full color image utilizing luminance gradients. U.S. Patent 5 382 976, Jan 1995.
25. K. Hirakawa and T.W. Parks. Adaptive homogeneity-directed demosaicing algorithm. *IEEE Trans. on IP*, 14(3):360–369, March 2005.
26. K. Hirakawa and P.J. Wolfe. Spatio-spectral color filter array for enhanced image fidelity. In *Proc. of International Conference on Image Processing*, 2007.

27. K. Hirakawa and P.J. Wolfe. Second generation cfa and demosaicking designs. In *SPIE Conf. on VCIP*, 2008.
28. J. F. Hamilton Jr. and J. E. Adams. Adaptive color plane interpolation in single color electronic camera. U.S. Patent 5 629 734, May 1997.
29. James E. Adams Jr. Design of practical color filter array interpolation algorithms for digital cameras part 2. In *ICIP (1)*, pages 488–492, 1998.
30. R. Kakarala and Z. Baharav. Adaptive demosaicking with the principal vector method. *IEEE Transactions on Consumer Electronics*, 48(4):932–937, Nov. 2002.
31. O. Kapah and H. Z. Hel-Or. Demosaicking using artificial neural networks. In *Proc. SPIE*, volume 3962, pages 112–120, 2000.
32. C.W. Kim and M.G. Kang. Noise insensitive high resolution demosaicking algorithm considering cross-channel correlation. In *Proc. ICIP*, pages III: 1100–1103, 2005.
33. Ron Kimmel. Demosaicking: image reconstruction from color ccd samples. *IEEE Transactions on Image Processing*, 8(9):1221–1228, 1999.
34. T. Kuno and H. Sugiura. Practical color filter array interpolation with constrained color correlation. *IEEE Trans. Consumer Electronics*, 52(3):896–903, August 2006.
35. C. Kwan and X. Wu. A classification approach to color demosaicking. In *Proc. ICIP*, pages IV: 2415–2418, 2004.
36. C. Laroche and M. Prescott. Apparatus and method for adaptively interpolating a full color image utilizing chrominance gradients. U.S. Patent 5 373 322, Dec 1994.
37. J. Lee, T. Jeong, and C. Lee. Edge-adaptive demosaicking for artifact suppression along line edges. *IEEE Transactions on Consumer Electronics*, 53(3):1076–1083, Aug. 2007.
38. W. Lee, S. Lee, and J. Kim. Cost effective color filter array demosaicking using spatial correlation. *IEEE Transactions on Consumer Electronics*, 52(2):547–554, May 2006.
39. X. Li. Blind image quality assessment. In *IEEE International Conference On Image Processing*, volume I, pages 449–452, 2002.
40. X. Li. Demosaicking by successive approximation. *IEEE Trans. on Image Proc.*, 14(2):370–379, 2005.
41. X. Li. Empirical bayesian image processing: Theory and applications. *IEEE Trans. on IP*, 2007. under review.
42. X. Li and M. Orchard. New edge directed interpolation. *IEEE Trans. on Image Proc.*, 10:1521–1527, 2001.
43. N.-X. Lian, L. Chang, Y.-P. Tan, and V. Zagorodnov. Adaptive filtering for color filter array demosaicking. *IEEE Transactions on Image Processing*, 16(10):2515–2525, 2007.
44. Yangjing Long and Yizhen Huang. Adaptive demosaicking using multiple neural networks. In *IEEE Signal Processing Society Workshop on Machine Learning for Signal Processing*, pages 353–357, 2006.
45. P Longere, X Zhang, PB Delahunt, and DH Brainard. Perceptual assessment of demosaicking algorithm performance. *Proc. of IEEE*, 90(1):123–132, Jan. 2002.
46. W. Lu and Y.P. Tan. Color filter array demosaicking: New method and performance measures. *IEEE Trans. on IP*, 12(10):1194–1210, October 2003.
47. R. Lukac, K. Martin, and K.N. Plataniotis. Demosaicked image postprocessing using local color ratios. *IEEE Trans. Cir. Sys. Video Tech.*, 14(6):914–920, June 2004.
48. R. Lukac and K.N. Plataniotis. A normalized model for color-ratio based demosaicking schemes. In *Proc. ICIP*, pages III: 1657–1660, 2004.
49. R. Lukac and K.N. Plataniotis. Data adaptive filters for demosaicking: a framework. *IEEE Transactions on Consumer Electronics*, 51(2):560–570, May 2005.
50. R. Lukac and K.N. Plataniotis. Demosaicking using vector spectral model. In *IEEE International Conference on Multimedia and Expo*, pages 1185–1188, July 2006.
51. R. Lukac, K.N. Plataniotis, D. Hatzinakos, and M. Aleksix. A novel cost effective demosaicking approach. *IEEE Transactions on Consumer Electronics*, 50(1):256–261, 2004.
52. David J. C. MacKay. Bayesian interpolation. *Neural Comput.*, 4(3):415–447, 1992.
53. H. S. Malvar, L.-W. He, and R. Cutler. High-quality linear interpolation for demosaicking of color images. In *Proc. IEEE Int. Conf. Acoustics, Speech and Signal Processing*, volume 3, pages 485–488, 2004.

54. D. Menon, S. Andriani, and G. Calvagno. Demosaicing with directional filtering and a posteriori decision. *IEEE Trans. on IP*, 16(1):132–141, Jan. 2007.
55. Daniele Menon and Giancarlo Calvagno. Demosaicing based on wavelet analysis of the luminance component. In *Proc. IEEE Int. Conf. Image Processing*, volume 2, pages 181–184, 2007.
56. J. Mukherjee, M.K. Lang, and S.K. Mitra. Demosaicing of images obtained from single-chip imaging sensors in yuv color space. *PRL*, 26(7):985–997, May 2005.
57. J. Mukherjee, R. Parthasarathi, and S. Goyal. Markov random field processing for color demosaicing. *PRL*, 22(3-4):339–351, March 2001.
58. D.D. Muresan and T.W. Parks. Demosaicing using optimal recovery. *IEEE Trans. on IP*, 14(2):267–278, February 2005.
59. Yoshikuni Nomura and Shree K. Nayar. A vq-based demosaicing by self-similarity. In *Proc. IEEE Int. Conf. Image Processing*, volume 3, pages 457–460, 2007.
60. I. Omer and M. Werman. Using natural image properties as demosaicing hints. In *Proc. ICIP*, pages III: 1665–1670, 2004.
61. Dmitriy Paliy, Vladimir Katkovnik, Radu Bilcu, Sakari Alenius, and Karen Egiazarian. Spatially adaptive color filter array interpolation for noiseless and noisy data. *International Journal of Imaging Systems and Technology*, 17(3):105 – 122, Oct. 2007.
62. S.C. Pei and I.K. Tam. Effective color interpolation in ccd color filter array using signal correlation. *CirSysVideo*, 13(6):503–513, June 2003.
63. Konstantinos N. Plataniotis and Anastasios N. Venetsanopoulos. *Color image processing and applications*. Springer-Verlag New York, Inc., New York, NY, USA, 2000.
64. J. Portilla, D. Otaduy, and C. Dorransoro. Low-complexity linear demosaicing using joint spatial-chromatic image statistics. In *Proc. ICIP*, pages I: 61–64, 2005.
65. R. Woods R. Gonzalez and S. Eddins. *Digital Image Processing Using MATLAB*. Prentice-Hall, 2004.
66. R. Ramanath and W. E. Snyder. Adaptive demosaicking. *Journal of Electronic Imaging*, 12(4):633–642, October 2003.
67. R. Ramanath, W. E. Snyder, G. L. Bilbro, and W. A. Sander III. Demosaicking methods for bayer color arrays. *Journal of Electronic Imaging*, 11(3):306–315, July 2002.
68. Chung-Yen Su. Highly effective iterative demosaicing using weighted-edge and color-difference interpolations. *IEEE Transactions on Consumer Electronics*, 52(2):639–645, May 2006.
69. D. Taubman. Generalized wiener reconstruction of images from colour sensor data using a scale invariant prior. In *Proc. IEEE Int. Conf. Image Processing*, volume 3, pages 801–804, 2000.
70. H.J. Trussell and R.E. Hartwig. Mathematics for demosaicking. *IEEE TIP*, 11(4):485–492, April 2002.
71. C.-Y. Tsai and K.-Tai Song. Heterogeneity-projection hard-decision color interpolation using spectral-spatial correlation. *IEEE Trans. Image Processing*, 16(1):78–91, January 2007.
72. C.Y. Tsai and K.T. Song. A new edge-adaptive demosaicing algorithm for color filter arrays. *IVC*, 25(9):1495–1508, September 2007.
73. P.P. Vaidyanathan. *Multirate Systems and Filter Banks*. Prentice Hall, Englewood Cliffs, New Jersey, 1993.
74. Xiaomeng Wang, Weisi Lin, and Ping Xue. Demosaicing with improved edge direction detection. In *International Symposium on Circuits and Systems*, pages 2048–2051, 2005.
75. X. Wu and N. Zhung. Primary-consistent soft-decision color demosaicking for digital cameras (patent pending). *IEEE Trans. on IP*, 13(9):1263–1274, September 2004.
76. W. Yu. Colour demosaicking method using adaptive cubic convolution interpolation with sequential averaging. *VISP*, 153(5):666–676, October 2006.
77. C.K.M. Yuk, O.C. Au, R.Y.M. Li, and Sui-Yuk Lam. Color demosaicking using direction similarity in color difference spaces. In *International Symposium on Circuits and Systems*, pages 1281–1284, 2007.
78. F. Zhang, X. Wu, X. Yang, and W. Zhang. Improved color demosaicing in weak spectral correlation. In *SPIE Conf. on VCIP*, 2008.
79. L. Zhang and X. Wu. Color demosaicking via directional linear minimum mean square-error estimation. *IEEE Trans. on IP*, 14(12):2167–2178, December 2005.
80. X. Zhang and B. A. Wandell. A spatial extension of cielab for digital color image reproduction. *SID Journal*. [Available online: <http://white.stanford.edu/~brian/scielab/scielab.html>], 1997.